Urban Ecosyst (2017) 20:497–509
DOI 10.1007/s11252-016-0610-9

Mapping forest structure and uncertainty in an urban area using leaf-off lidar data

Huan Gu [1,2] · **Philip A. Townsend** [1]

Published online: 29 October 2016

Abstract Forests are important to nutrient cycling, hydrology, climate and aesthetics in urban ecosystems. Effective forest management in urban environments requires detailed data on the spatial distribution and structure of urban forests, but the lidar which are best for mapping the complexity of these forests are often unavailable or prohibitively expensive for municipalities. However, leaf-off small footprint lidar originally collected for topographic mapping are increasingly available, and will soon become accessible to forest managers in the U.S. through 3DEP (3D Elevation Program). In this paper, we demonstrated the opportunistic use of existing leaf-off lidar to map forest structure and associated uncertainties in Madison, Wisconsin and neighboring municipalities. Using empirical models, we were able to map five structural variables and aboveground biomass with accuracies comparable to or better than other studies using comparable data and with errors generally <20 % of the data range. Highest uncertainties in our forest structure maps occurred in residential neighborhoods and along forest edges. From the results, we present maps of forest structure and, to our knowledge, first of a kind pixel-wise uncertainty maps for an urban area. These maps provide the basis for a spatially comprehensive assessment of forest resources and are effective for urban inventory and change assessment. For example, the maps enabled comprehensive comparison of carbon storage by urban trees among cities, with a range in our study of 1.2 kg/m^2 to 5.6 kg/m^2, and with major variations due to differences in city development patterns and ages.

Keywords Urban forests · Forest structure · Uncertainty · Leaf-off lidar · Carbon storage

✉ Huan Gu
hgu6@wisc.edu; guhuan114031@gmail.com

[1] Department of Forest and Wildlife Ecology, University of Wisconsin-Madison, 1630 Linden Drive, Madison, WI 53706, USA

[2] Graduate School of Geography, Clark University, 950 Main Street, Worcester, MA 01610, USA

Introduction

Urban forests play an important role in offsetting environmental impacts of urbanization by providing a range of ecosystem services. Urban trees sequester carbon through photosynthesis and storage of carbon as tree biomass (Nowak and Crane 2002). Urban trees also decrease stormwater runoff by intercepting rainwater on leaves, branches, and trunks (Bolund and Hunhammar 1999), reduce nutrient export, particularly nitrogen and phosphorus, through root uptake (Day et al. 2010), and increase biodiversity by providing habitat and food resources to insects, birds and a wide variety of wildlife (Alvey 2006; Savard et al. 2000). Quantification and mapping of urban forest structure are needed to inventory and understand their spatial patterns, and then to maximize the benefits of urban ecosystems through management or planning (McPherson et al. 1997).

Many municipalities have been inventorying forest structure since at least the 1980s (Nowak et al. 2013). However, traditional field sampling is labor-intensive, time-consuming and expensive (Myeong et al. 2006). Remote sensing data are capable of making horizontal and vertical measurements over large areas in an efficient and timely way. Multispectral and hyperspectral remote sensing having difficulty penetrating beyond canopy layers are better suited for mapping horizontal structure (Hyde et al. 2006; Swatantran et al. 2011). Interferometric synthetic

aperture radar (InSAR) is best suited for structurally homogeneous forest types (Hyde et al. 2006; Hyde et al. 2007). Lidar (light detection and ranging) has shown great advantages to measure structural and biophysical properties more accurately (Lefsky et al. 2002). Key variables that have been derived from discrete-return lidar to estimate forest biophysical parameters in natural forests include aboveground biomass, basal area, diameter, height, crown length, crown width, stand density, wood volume and leaf area index (Lim et al. 2003; Næsset 2004; Popescu et al. 2004; Bortolot 2006; Morsdorf et al. 2006; Farid et al. 2008; Hudak et al. 2008; García et al. 2010; Hawbaker et al. 2010; Korhonen et al. 2011; Muss et al. 2011; Gleason and Im 2012). However, the development of methods to quantify forest structure and biophysical status in urban forests using lidar data has lagged work in natural forests due to complexity of urban forests, including high levels of fragmentation, the presence of a large number of exotic species, and active management (Hope et al. 2003). Given the heterogeneity and complexity of trees in urban landscapes, very high point-density lidar data were mostly used to estimate structural variables of individual tree in urban forests (Moskal and Zheng 2012; Shrestha and Wynne 2012; Omasa et al. 2008). Very high point-density data can provide accurate tree-level quantification of biophysical variables of urban forests. However, such data are limited by coverage area thus missing comprehensive mapping ability, and add cost and computation complexity to the mapping process. In contrast, though low point-density lidar data can only estimate structural variables at area level, they provide a basis for a spatially comprehensive assessment of urban forest resources, filling the gaps in our current inventories of urban forests over large areas.

For mapping forest structure, lidar data are optimally collected under leaf-on conditions, while leaf-off lidar are preferred for ground detection needed to map elevation (Anderson et al. 2005). Although leaf-off lidar are not ideal for forest characterization, it has been demonstrated to be useful dataset for estimating forest structure (Anderson and Bolstad 2013; Hawbaker et al. 2010; Næsset 2005), because more laser pulses penetrate through leafless canopies, providing greater information on vertical structure in deciduous forests than leaf-on lidar (Brandtberg et al. 2003). For urban forest managers, budgets are often limited, and widespread leaf-on lidar suitable for forest characterization are costly to acquire and process. However, the 3DEP (3D Elevation Program 2014) in U.S. will make national-wide high-quality lidar data available within 8 years to support topographic mapping activities addressing climate resilience, and much of those lidar data have been collected during leaf-off seasons. The widespread availability of high-quality lidar from 3DEP makes it a potentially invaluable tool for applications in urban ecosystem assessment and management.

In this paper, we are motivated by the desire to make use of existing lidar originally collected for topographic mapping to characterize forest structure and aboveground biomass in an urban area. Although not optimal, existing lidar provides an ***opportunistic*** data source to characterize forest structure (Hawbaker et al. 2010). By including uncertainty analysis and mapping, we can provide locations where estimates are more confident and reliable to city foresters and other users. These uncertainties in forest structure estimated from lidar result from limitations imposed by field sampling and allometric scaling (Frazer et al. 2011), remote sensing data acquisition and processing (Lu et al. 2012), and from the regression models of biomass as a function of lidar derived variables (Gonzalez et al. 2010). Statistical methods have been proposed to analyze uncertainties in estimating biomass or carbon density from lidar data, such as Monte Carlo simulation (Frazer et al. 2011; Gonzalez et al. 2010). Here we show an approach to calculate uncertainty, which can then be mapped as absolute or percent errors, and map uncertainty in practice. Therefore, our objectives in this paper are to: (1) demonstrate the use of existing discrete-return leaf-off lidar to quantify forest structure in an urban area; (2) map forest structure variables and associated uncertainty using developed empirical models; and (3) summarize and compare aboveground biomass and carbon stock in seven municipalities with different land uses and development histories in the study area.

Methods

Study area

The study was conducted in City of Madison and neighboring municipalities and suburban areas in southern central Wisconsin, USA (Fig. 1). The topography in this area is flat with elevation ranging from 258 m to 346 m. This region is comprised of a diverse mix of deciduous and evergreen trees, with dominants including white oak (*Quercus alba*), red oak (*Quercus rubra*), sugar maple (*Acer saccharum*), silver maple (*Acer saccharinum*), red pine (*Pinus resinosa*) and white pine (*Pinus strobus*) (Gu et al. 2015). Urban forests in the study area occur in a variety of settings with varying extent of human interaction and management, such as the University of Wisconsin Arboretum (A on Fig. 1a), nature preserves (B on Fig. 1a), city parks, trees in streets and residential backyards (A and B in Fig. 1a), and natural forests surrounded by the agriculture matrix at the suburban-to-rural interface (C on Fig. 1a). The study area comprises seven major municipalities, all with differing land use, land cover, development and management policies (Fig. 1b).

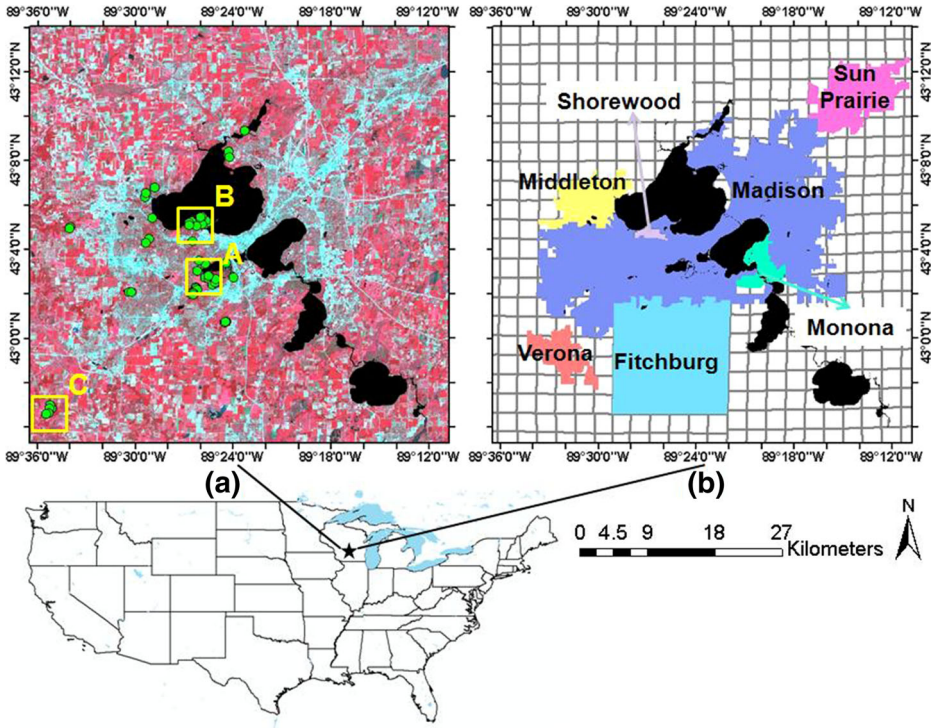

Fig. 1 Study area in Dane County, Wisconsin, USA. **a** *Green dots* show locations of field plot centers, and *yellow boxes* refer to areas shown on maps in Fig. 4; **b** *Grey grids* are lidar tiles, seven polygons are the major municipalities within the study area, with results summarized in Table 5

Field data

Forest measurements were made for 60 plots covering the range of stand structure and species composition in the study area. All the plots were established in urban forest patches of continuous canopy cover with areas larger than 0.25 ha and exhibiting the range of stand density, species composition and structure found in the study area. Each plot consisted of 5 subplots arranged in a cruciform layout following Townsend (2002), with a distance of 25 m between the intersection (plot center) and four end points. At each subplot, all live and dead trees recorded as "in" using a metric basal area factor (BAF) 2 prism were identified to species, and diameter at breast height (dbh) was recorded. Aboveground biomass per unit area at each subplot was estimated using a standard allometric approach based on a variable-sized plot design (Grosenbaugh 1952; Grosenbauch 1958): (1) Determine the maximum distance (D_{max}) that a tree of a given dbh counted as "in" (Eq. 1). (2) Determine the number of trees (Density) of this dbh that would be found per unit area (ha) (Eq. 2). (3) Estimate tree biomass (Bm) by applying Jenkin's dbh-based species-specific allometric equations (Jenkins et al. 2004) (Eq. 3). (4) Estimate biomass per unit area ($BmpA_{tree}$) of this tree (Eq. 4). (5) Sum biomass per unit area across for all the tallied trees within this subplot to get a total biomass per unit area in this subplot ($BmpA_{subplot}$, Eq. 5). Basal area per subplot ($BA_{subplot}$) was calculated by 2 (BAF) multiplying number of sampled trees within the subplot (n) (Eq. 6). We averaged aboveground biomass, basal area and tree diameter from 5 subplots to obtain plot-level aboveground biomass (AGB), basal area (BA), mean tree diameter (DBH). Additional measurements included tree height, crown base height and crown width of all the tallied trees at the plot center subplot using a Haglöf Vertex Laser VL402 hypsometer (Haglöf Sweden AB, Långsele, Sweden). Crown length was calculated by the difference of canopy height and crown base height. We averaged tree height, crown length and crown width to obtain plot-level mean canopy height (Ht), mean crown length (CL), and mean crown width (CW).

$$D_{max} = \sqrt{0.25 * dbh^2/BAF} \quad (1)$$

$$Density = 10000/\pi D_{max}^2 \quad (2)$$

$$Bm = f(dbh) \quad (3)$$

$$BmpA_{\text{tree}} = Bm * Density \quad (4)$$

$$BmpA_{\text{subplot}} = \sum BmpA_{\text{tree1}} + BmpA_{\text{tree2}} + \cdots + BmpA_{treen} \quad (5)$$

$$BA_{\text{subplot}} = BAF * n \quad (6)$$

Lidar data

The county-wide lidar collection was contracted by the Dane County Land Information Office to develop a high resolution county-wide digital elevation model (DEM). Ayres Associates

(www.ayresassociates.com) used a 1064 nm Leica ALS70 laser scanner with scan rate of 69.00 Hz and scan angle between -17° and +18°, and flew at an altitude of 1750 m above ground level with flight speed of 248.40 km/h during leaf-off conditions in April, 2009, producing discrete-return point clouds with a point density of 1 point per square meter (ppm). Ayres processed the raw data to remove spurious points, calibrate heights caused by scan angle effects and calibrate intensity caused by range differences, and generated point clouds and 3 m DEM data products for the whole county. Point cloud data included coordinates, height, intensity, scan angle and class (e.g. ground, vegetation, building and water). Relative height for each point record was obtained by differencing return height and DEM in R 3.0.2 (R Development Core Team 2013).

Since our field plots used a variable-sized plot design with no fixed boundary, we tested six footprint radii from which we generated lidar metrics at each plot center: 10 m, 15 m, 20 m, 25 m, 30 m and 35 m. For each field-sampled plot and each footprint radius, we derived metrics from relative height and intensity of lidar (Table 1), including quantiles (Qxx_H, Qxx_I, where xx refers to xx% quantile), maximum (Max_H, Max_I), mean (Mean_H, Mean_I), standard deviation (Std_H, Std_I), coefficient of variation (CV_H, CV_I), kurtosis (Kurt_H, Kurt_I) and skewness (Skew_H, Skew_I) of lidar relative height (H) and intensity (I). Additional variables derived from relative height only included the difference between tallest height and 25 %, 50 % and 75 % quantiles (Diff_Max_H_Q25_H, Diff_Max_H_Q50_H, Diff_Max_H_Q75_H) (García et al. 2010); and PCan, the proportion of canopy returns (heights larger than 1.4 m) to all the returns (Morsdorf et al. 2006). Point returns with relative height less than 1.4 m were excluded from the calculation of all metrics except for PCan, because trees were measured at breast height and because laser pulse penetration at the bottom of canopy is known to be highly variable (Wasser et al. 2013).

Data analysis

Ordinary least squares (OLS) regression was used to develop predictive models between forest structure measurements (AGB, BA, DBH, Ht, CL and CW) and lidar-derived metrics (Table 1). Potential explanatory variables were assessed using forward model selection until the addition of new variables provided no improvement of model performance. All the selected explanatory variables were significant (p-value <0.05), and correlation coefficients among explanatory variables were also evaluated to ensure that included predictors in the models had low collinearity ($r < 0.5$). Aside from canopy height, all response variables were natural log normalized for statistical analysis to ensure normal distribution.

We applied cross-validation by jack-knifing our dataset 1000 times using a random 75 % of the dataset ($N = 45$) to build linear model and testing on the remaining 25 % of samples for validation ($N = 15$). We reported R^2, root mean squared error (RMSE), and relative RMSE of

Table 1 Description of predictor variables derived from lidar height and intensity within a footprint

	Variable	Description
Height metrics	Q*xx*_H	Height of the xx*th* quantile (10*th*, 20*th*, 30*th*, 40*th*, 50*th*, 60*th*, 70*th*, 80*th*, 90*th*)
	Max_H	Maximum height
	Mean_H	Mean height
	Std_H	Standard deviation of height
	CV_H	Coefficient of variation of the height
	Kurt_H	Kurtosis of the height
	Skew_H	Skewness of the height
	Diff_Max_H_Q*25*_H	Height difference between largest and 25*th* quantile
	Diff_Max_H_Q*50*_H	Height difference between largest and 50*th* quantile
	Diff_Max_H_Q*75*_H	Height difference between largest and 75*th* quantile
	PCan	Proportion of canopy returns to all returns
Intensity metrics	Q*xx*_I	Intensity of the xx*th* quantile (10*th*, 20*th*, 30*th*, 40*th*, 50*th*, 60*th*, 70*th*, 80*th*, 90*th*)
	Max_I	Maximum intensity
	Mean_I	Mean intensity
	Std_I	Standard deviation of intensity
	CV_I	Coefficient of variation of the intensity
	Kurt_I	Kurtosis of the intensity
	Skew_I	Skewness of the intensity

Table 2 Average of stand structure variables by cover type for field measured plots

Dominant species	Scientific name	Common name	AGB (Mg/ha)	BA (m^2/ha)	DBH (cm)	Ht (m)	CL (m)	CW (m)
QURU	*Quercus rubra*	Red oak	221.00	28.40	53.26	24.60	17.86	14.36
QUAL	*Quercus alba*	White oak	170.52	22.58	46.61	23.74	15.63	14.02
QUMA	*Quercus macrocarpa*	Bur oak	157.94	22.40	49.41	16.64	11.54	19.16
ACSM	*Acer saccharum*	Sugar maple	232.67	25.55	48.96	25.68	18.24	15.40
ACSN	*Acer saccharinum*	Silver maple	173.55	25.20	63.12	26.54	21.96	18.62
CAOV	*Carya ovata*	Shagbark hickory	187.93	23.00	36.92	22.90	16.68	12.95
PRSE	*Prunus serotina*	Black cherry	155.39	22.80	32.30	20.88	15.18	9.52
FRAM	*Fraxinus americana*	White ash	158.25	25.60	43.25	20.36	19.36	7.69
JUNI	*Juglans nigra*	Black walnut	98.48	16.80	44.68	26.26	19.88	11.99
ROPS	*Robinia pseudoacacia*	Black locust	192.10	31.60	37.20	29.35	22.25	11.17
CEOC	*Celtis occidentalis*	Northern hackberry	118.10	20.40	32.37	17.86	12.76	8.50
TIAM	*Tilia americana*	Basswood	182.73	26.40	47.77	29.62	25.72	15.37
PODE	*Populus deltoides*	Eastern cottonwood	125.94	35.20	49.86	30.73	17.28	11.93
LITU	*Liriodendron tulipifera*	Tulip poplar	237.64	32.80	58.37	27.70	14.76	13.41
PIRE	*Pinus resinosa*	Red pine	145.04	38.76	26.84	19.26	7.62	5.63
PIST	*Pinus strobus*	White pine	138.41	37.80	37.74	24.58	13.07	7.69
PISY	*Pinus sylvestris*	Scots pine	181.08	32.80	34.34	24.60	20.42	6.63
JUVI	*Juniperus virginia*	Red cedar	180.38	34.00	24.30	15.06	11.55	8.79
THOC	*Thuja occidentalis*	White cedar	118.47	34.00	30.28	20.34	11.02	7.38
PIAB	*Picea abies*	Norway spruce	145.65	26.40	35.60	24.88	14.28	8.57
Data range			84.41- 277.59	16.80- 47.60	22.39- 83.18	15.06- 33.70	4.94- 27.23	4.13- 23.55

prediction on both calibration and validation datasets in back-transformed scale by exponential calculation if the variables were log transferred. Models with lower differences between validation and calibration diagnostics are considered more stable than those with larger differences. All analyses were conducted in R 3.0.2 (R Development Core Team 2013).

Forest structure and uncertainty mapping

Maps of forest structure were generated from the lidar data by superimposing a grid (20 m spacing) with a sufficient number of lidar returns to calculate a statistical distribution per cell, calculating the lidar metrics in Table 1 for all the cells, and then applying the regression equations for the structural attributes (AGB, BA, DBH, Ht, CL and CW) to each cell. The lidar metrics were only synthesized from lidar returns that had been recorded as vegetation in the LAS dataset provided by Ayres.

In addition, for each structural variable we mapped pixel-wise uncertainty in the structural estimates. Our pixel estimates of uncertainty are calculated as ***percent uncertainty*** by dividing the length of 95 % confidence interval by the pixel-wise prediction (Eq. 7).

$$Percent\ \ uncertainty = 100 * (SV_{97.5} - SV_{2.5}) / SV_{prediction} \quad (7)$$

SV refers to a given structural variable, i.e. AGB, BA, DBH, Ht, CL or CW. This is a conservative estimate of uncertainty, encompassing the range of uncertainty both minus and plus the pixel-wise prediction. Such an approach is required because of the log transformation applied to 5 of the 6 structural variables, in which lower

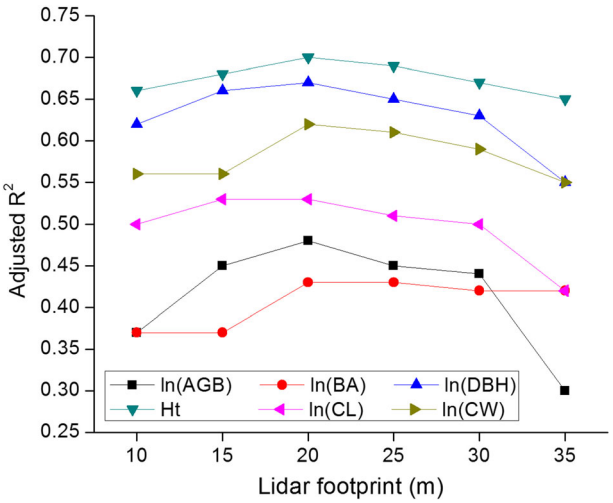

Fig. 2 Cross-validated adjusted R^2 for estimating forest structure variables across 6 different footprints. AGB is aboveground biomass, BA is basal area, DBH is average diameter at breast height, Ht is tree height, CL is crown length and CW is crown width

Table 3 Final models, mean adjusted R^2, mean RMSE and relative RMSE of 75 % training and 25 % validation data for estimating forest structure variables

Forest structure variable*	Model	Training data (75 %)			Validation data (25 %)		
		Mean adjusted R^2	Mean RMSE**	Relative RMSE ***	Mean adjusted R^2	Mean RMSE	Relative RMSE
ln(AGB)	Skew_I + Q50_H	0.51	32.91	19.33 %	0.48	30.97	18.19 %
ln(BA)	PCan +CV_H	0.61	4.87	16.31 %	0.59	4.67	15.64 %
ln(DBH)	Q80_H+ PCan	0.73	6.32	14.93 %	0.71	5.88	13.90 %
Ht	Q90_H	0.71	2.22	9.36 %	0.70	2.09	8.81 %
ln(CL)	Q80_H+ PCan +Kurt_H	0.59	3.46	22.77 %	0.55	3.39	22.31 %
ln(CW)	Q70_I + Max_I	0.64	2.72	23.76 %	0.62	2.59	22.63 %

* Forest structure variables are aboveground biomass (AGB, Mg/ha), basal area (BA, m^2 /ha), diameter at breast height (DBH, cm), canopy height (Ht, m), crown length (CL, m) and crown width (CW, m)

**Mean RMSE are reported as back-transformed RMSE

***Relative RMSE are calculated by Mean RMSE/mean of forest structure variables

95 % uncertainties in the original unit of a variable are smaller than upper 95 % uncertainties. All calculations were initially performed on a lidar-tile basis, and were combined into a single dataset in R. Then, we gridded the dataset to raster images of structural estimates and uncertainty for each variable at the cell size of 20 m using ArcMap 10.1 (ESRI 2012).

Carbon storage by urban trees

We estimated total aboveground biomass and standard error by municipality from the forest structure maps by summation of aboveground biomass and associated standard error for all the forest pixels within each municipality boundary (Fig. 1b). We also approximated total biomass by applying root-to-shoot ratio of 0.26 to total aboveground biomass (Cairns et al. 1997), and total carbon storage was estimated by multiplying total biomass by carbon content fraction of 0.5 (Nowak and Crane 2002).

Results

The study area consisted of forests dominated by 20 different species, including 14 deciduous types and 6 evergreen types (Table 2). Forests exhibited a wide range of structural characteristics, with canopy height (Ht) ranging from 15.06 to 33.70 m and aboveground biomass (AGB) from 84.41 to 277.59 Mg/ha. Additional structural variables including basal area (BA), mean diameter at breast height (DBH), crown length (CL) and crown width (CW) are summarized in Table 2.

Table 4 Final models and model coefficients for estimating forest structure variables.

Forest structure variable*	Model	β_0**		β_1		β_2		β_3	
		Mean	Std	Mean	Std	Mean	Std	Mean	Std
ln(AGB)	Skew_I + Q50_H	4.18	0.090	0.19	0.022	0.04	0.005		
ln(BA)	PCan +CV_H	2.79	0.087	1.07	0.095	-1.23	0.114		
ln(DBH)	Q80_H+ PCan	3.13	0.091	0.05	0.003	-0.63	0.079		
Ht	Q90_H	3.90	0.747	0.90	0.035				
ln(CL)	Q80_H+ PCan +Kurt_H	2.12	0.163	0.06	0.005	-0.79	0.143	-0.03	0.007
ln(CW)	Q70_I + Max_I	2.62	0.055	-0.06	0.004	0.01	0.002		

* Forest structure variables are aboveground biomass (AGB, Mg/ha), basal area (BA, m^2 /ha), diameter at breast height (DBH, cm), canopy height (Ht, m), crown length (CL, m) and crown width (CW, m)

** β_0, β_1, β_2 and β_3 are coefficients of the linear models, β_0 is the coefficient of constant, β_1, β_2 and β_3 are the coefficients of selected predictor variables. For example: the model of AGB is ln(AGB) = β_0 + β_1* Skew_I + β_2* Q50_H

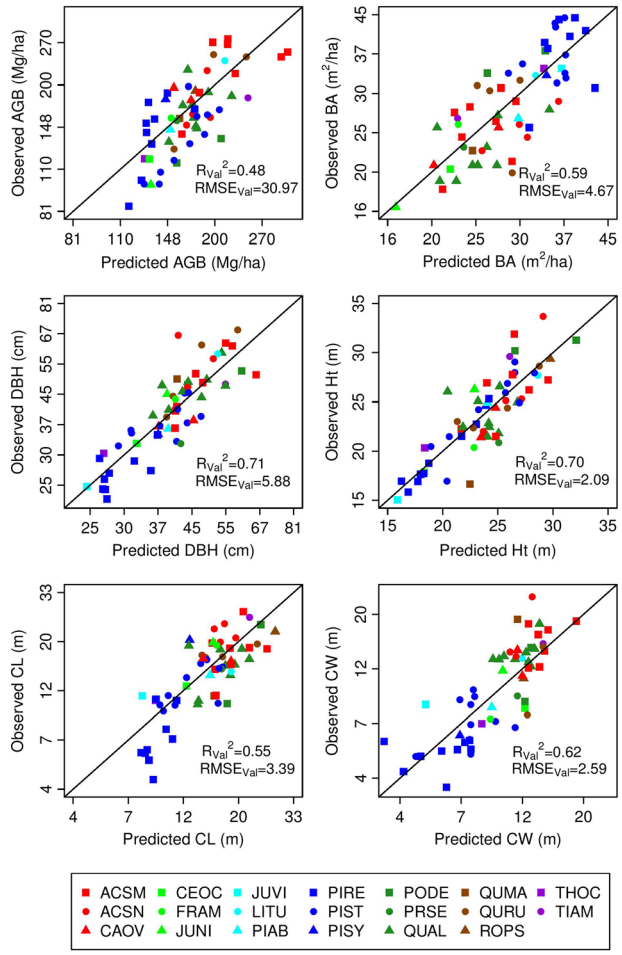

Fig. 3 Linear regression results for six forest structure variables using final models, with point symbols varied by dominant species. Species codes are listed in Table 2

Lidar footprint radius for plots

We found a consistent pattern of increasing R^2 and decreasing RMSE in predicting structural variables up to a 20 m radius footprint for calculating lidar metrics, and leveling off or decreasing to 35 m (Fig. 2). Specifically, R^2 increased by 3 % to 11 % for different structural variables as lidar footprint increased from 10 m to 20 m, and decreased by 1 % to 18 % as footprint increased from 20 m to 35 m. Based on this result, all the subsequent analyses employed the 20 m radius footprint to compute lidar metrics for our field plots.

Forest structure models

Model performance and selected predictor variables varied considerably among the different structural parameters (Table 3). Of six structural variables, canopy height was predicted best using 90th percentile height (validation: R^2 = 0.70, RMSE = 2.09 m, relative RMSE = 8.81 %), while aboveground biomass performed most poorly (validation: R^2 = 0.48, RMSE = 30.97 Mg/ha, relative RMSE = 18.19 %). Models for six forest structural variables were employed to generate maps of forest structure using mean beta coefficients derived from the 1000 models fitted with randomly drawn 75 % subset of the data (Table 4, Fig. 3). For R^2, RMSE and beta coefficient distribution of 1000 developed linear models, see details in Gu (2015).

Maps of forest structure and uncertainty

Maps of canopy height, crown width and aboveground biomass (Fig. 4, first three rows) show the considerable variations in forest structure within areas A, B and C indicated by Fig. 1a. Maps of uncertainty in aboveground biomass (Fig. 4, bottom row) illustrate that highest levels of mapped uncertainty occur on the edge of forest patches and in heavily treed neighborhood areas where forest cover is discontinuous and lidar returns from trees are irregular. Across the whole study area, the length of 95 % confidence interval in pixel-wise mean aboveground biomass varied from 16.0 to 88.8 Mg/ha, averaging 30.3 ± 12.7 Mg/ha, with the majority of pixels (73 %) in the study area having uncertainties in per pixel aboveground biomass that are within -17 % to +20 % of the predicted values.

Carbon stocks in municipalities

One utility of this work is the ability to provide an accounting of total aboveground biomass plus uncertainty in its estimate, as well as total carbon storage and carbon stock per unit of land in the seven municipalities within the study area (Table 5). For example, over the 207.3 km^2 of land area for City of Madison, we estimated a total aboveground biomass of 1.0 million Mg with uncertainty range of 0.9 to 1.2 million Mg, and total carbon storage by urban trees of 0.7 million Mg averaging 3.2 kg/m^2 carbon. Estimated total aboveground biomass for the seven municipalities is 1.6 million Mg with an uncertainty range of 1.4 to 1.9 million Mg, or approximately uncertainty of -14 % to +16 %.

Discussion

Increasing the value of existing lidar datasets

We employed existing leaf-off discrete return lidar data to map urban forest structure. Although leaf-on data are most often acquired for forestry management, it is unlikely that most municipalities can justify the expense of collecting lidar data specifically for mapping forest structure. However, leaf-off lidar data are regularly acquired to detect bare ground for topographic mapping, floodplain delineation (Hodgson et al. 2005) and urban infrastructure mapping. A considerable

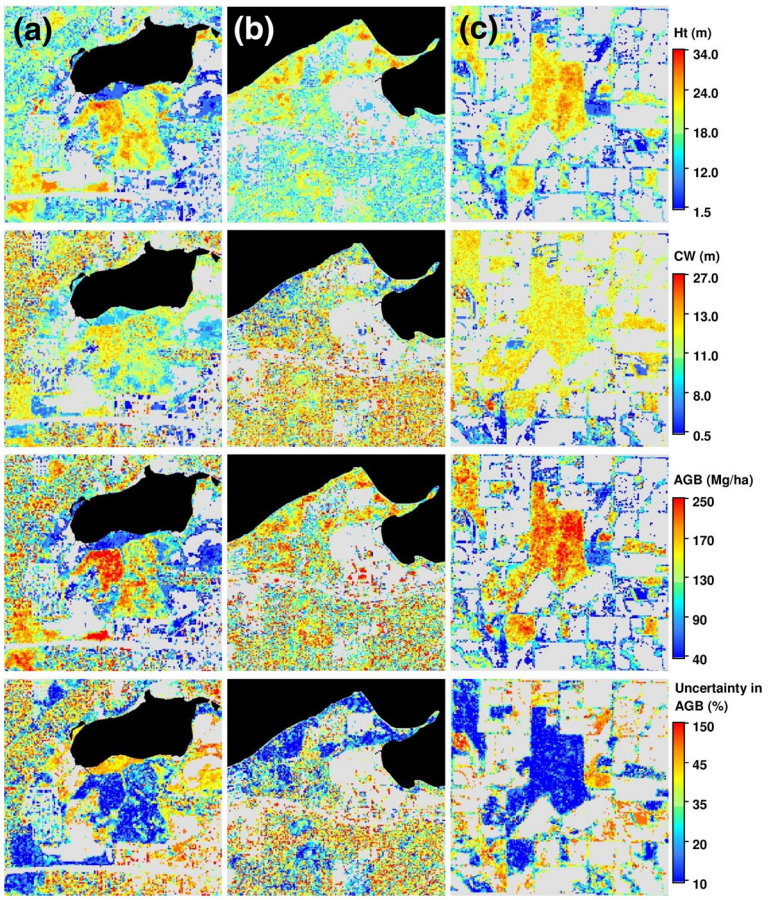

Fig. 4 Forest structure maps for areas **a, b, c** in Fig. 1a (by column). *Top row* is canopy height (Ht, m); *second row* is crown width (CW, m); *third row* is aboveground biomass (AGB, Mg/ha); and the *fourth row* is the uncertainty (% in the length of 95 % confidence interval to the estimate) in aboveground biomass

amount of value can be added to such "opportunistic" datasets if they can be used to estimate properties beyond their intended uses, such as merchantable volume (Hawbaker et al. 2010) and bird species richness (Lesak et al. 2011). Although leaf-off data pose some challenges in areas with mixed deciduous and evergreen forests, we addressed this by including variable Skew_I that capture differences between conifers and leaf-off deciduous forests (Fig. 5a).

Maps of forest structure from leaf-off lidar in urban areas provide the basis for a spatially comprehensive assessment of forest resources. Aboveground biomass maps offer opportunities to evaluate and update existing national biomass and carbon datasets (NBCD, Kellndorfer et al. 2013), and reduce the uncertainties in areas where forest inventory and analysis (FIA) sampling has not been deployed. Moreover, urban tree inventories conducted by municipalities are usually incomplete, usually covering a small portion of the forested area of a city (Nowak et al. 2013), yet the benefits of complete spatial coverage provided by lidar maps could substantially improve urban ecosystem management. For example, in Wisconsin

Table 5 Summary of total aboveground biomass (AGB), uncertainty range of total aboveground biomass, total carbon stock, aboveground biomass per unit of land and carbon stock per unit of land in the seven municipalities shown in Fig. 1b

City	Area (ha)	Total AGB (10^3 Mg)	Uncertainty Range* (10^3 Mg)	Total carbon stock (10^3 Mg)	AGB per area (Mg/ha)	Carbon stock per area (kg/m^2)
Madison	20,730	1047	904 – 1217	660	50.5	3.2
Shorewood	208	18	16– 21	12	88.4	5.6
Middleton	2098	65	57– 74	42	30.8	1.9
Monona	852	52	46– 60	33	61.2	3.9
Verona	1453	27	23– 30	17	18.3	1.2
Fitchburg	9106	310	270 – 357	195	34.0	2.1
Sun Prairie	3224	96	81 – 115	61	29.9	1.9
Total	37,672	1615	1397– 1873	1018	42.9	2.7

*Uncertainty range is defined by the 95 % confidence interval of the prediction from AGB model

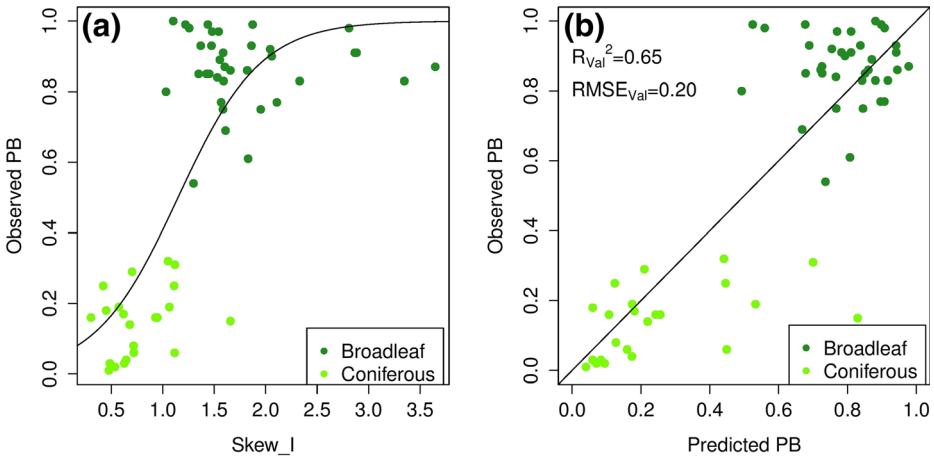

Fig. 5 Logistic regression results for estimating proportion of broadleaf (PB) using 20 m footprint lidar. **a** Plots observed PB vs. Skew_I (skewness of intensity), and a fitted logistic regression curve; **b** The regression result of estimating PB using Skew_I and Kurt_I (kurtosis of intensity)

and other areas of the Upper Midwest U.S., the ability to quantify forest aboveground biomass has significant management implications in light of ongoing threats from invasive species such as the emerald ash borer (EAB, Poland and McCullough 2006). It is estimated that 20 % of the tree biomass in the Madison area is in ash trees (Marla Eddy, city forester, personal communication), which could equate more than 209,000 metric tons of ash wood that will have to be disposed of locally if proactive management efforts to remove ash trees are implemented. In addition, maps of other forest structural variables, especially canopy height, crown width and crown length, provide information to characterize important determinants of tree species composition (Gu et al. 2015), bird diversity (Lesak et al. 2011) and wildlife habitat (Hyde et al. 2006) in the urban environment. Spatial maps of urban forests could enable social scientists to investigate public health and understand epidemic distribution patterns in urban community (Lovasi et al. 2013). Finally, these structural maps may be also relevant to understanding energy usage and urban heat island effects (Akbari et al. 2001).

Empirical models to predict forest structure

We employed empirical models to map forest structure from lidar. This was necessary due to the opportunistic nature of the lidar data available to us. The variables we selected were comparable to other studies, for example, Q50_H was used to estimate aboveground biomass in pine dominated forests in central Spain (García et al. 2010), upper canopy quantiles (Q90_H and Q80_H) were significant to predict diameter, canopy height and crown length in deciduous and evergreen forests in Wisconsin (Hawbaker et al. 2010; Muss et al. 2011). However, we identified skewness of leaf-off intensity (Skew_I) as an important metric to estimate aboveground biomass from leaf-off lidar. Skew_I is a new useful metric for leaf-off lidar, which was not reported in previous studies of forest structure characterization. As well, we found that Skew_I from leaf-off lidar was strongly correlated with forest physiognomic composition (broadleaf deciduous vs. coniferous evergreen), which alone explained 48 % of the variance in the proportion of the basal area on a plot consisting of deciduous trees (Fig. 5a). Together with two other significant variables, CV_I and Kurt_I (Table 1), we found that intensity data facilitated prediction of the proportion of deciduous trees with a fit of R^2_{val} = 0.65, $RMSE_{val}$ = 0.20 (Fig. 5b). This points to another utility and value of the 3DEP leaf-off lidar that will be soon widely available across the United States. Although 3DEP is an activity to bring together locally collected lidar datasets into a national database for high-resolution elevation mapping, the data could also be purposed for canopy structure mapping in urban areas.

Comparison to other research

Our results compare favorably to other studies that used discrete-return small-footprint lidar to estimate plot-level forest structure in natural forests (Table 6), with our R^2_{val} falling within the range of model performance in the literature and slightly better for crown length. Moreover, our analyses employed a rigorous calibration/validation procedure that may have decreased our diagnostic statistics relative to other studies reported in the literature.

Our results are especially encouraging given that the study was conducted in urban forests, which are considerably more heterogeneous than natural forests, especially the plantations and other working forests where the majority of lidar studies have been conducted. Specifically, tree composition is much more diverse in urban forests (Alvey 2006) because urban trees are often planted and frequently managed. Tree species for planting or retention are selected for a variety of functions, e.g. growth rate, climate, tolerance and aesthetics, resulting in a larger proportion of exotic species. We tallied 44 tree species in our

Table 6 Results of estimating plot-level forest structure variables using small footprint discrete lidar from other studies

Forest structure variable*	Forest type	N of species	N of plots	R^2	Estimated error	Unit	Reference
AGB	Conifer, hardwood	20	60	0.40-0.48	30.97-33.52[a]	Mg/ha	The authors
	Conifer, hardwood	N/A	18	0.22-0.93	17.65-44.25[a]	Mg/ha	Gleason and Im (2012)
	Conifer, hardwood	9	148	0.72-0.75	70.42-74.03[a]	Mg/ha	Muss et al. (2011)
	Conifer	3	45	0.58-0.67	28.89-34.09[a]	Mg/ha	García et al. (2010)
	Conifer	1	25	0.04-0.62	12.40-214.8[a]	Mg/ha	Bortolot (2006)
	Hardwood	3	33	0.09-0.33	45.46-51.08[a]	Mg/ha	Popescu et al. (2004)
	Conifer	3	31	0.78-0.82	33.25-41.55[a]	Mg/ha	Popescu et al. (2004)
	Hardwood	2	49	0.78-0.85	0.46-0.55[b]	Mg/ha	Lim et al. (2003)
BA	Conifer, hardwood	20	60	0.43-0.59	4.67-5.46[a]	m^2/ha	The authors
	Conifer, hardwood	9	31	0.46-0.48	8.12-8.31[a]	m^2/ha	Muss et al. (2011)
	Conifer, hardwood	6	114	0.43-0.46	-20.56-18.12[c]	m^2/ha	Hawbaker et al. (2010)
	Hardwood	3	33	0.25	6.47[a]	m^2/ha	Popescu et al. (2004)
	Conifer	3	31	0.74-0.76	5.66-6.94[a]	m^2/ha	Popescu et al. (2004)
	Conifer, hardwood	3	116	0.74-0.94	0.13-0.22[d]	m^2/ha	Næsset (2004)
	Hardwood	2	49	0.82-0.88	0.39-0.47[b]	m^2/ha	Lim et al. (2003)
DBH	Conifer, hardwood	20	60	0.66-0.71	5.88-6.26[a]	cm	The authors
	Conifer, hardwood	9	31	0.61-0.64	5.97-6.16[a]	cm	Muss et al. (2011)
	Conifer, hardwood	6	114	0.45-0.48	-10.40-6.90[c]	cm	Hawbaker et al. (2010)
	Hardwood	3	33	0.41-0.51	5.80-6.49[a]	cm	Popescu et al. (2004)
	Conifer	3	31	0.70-0.90	4.42-7.03[a]	cm	Popescu et al. (2004)
	Conifer, hardwood	3	116	0.55-0.69	0.12-0.17[d]	cm	Næsset (2004)
	Hardwood	2	49	0.37-0.63	0.14-0.19[b]	cm	Lim et al. (2003)
Ht	Conifer, hardwood	20	60	0.68-0.70	2.09-2.17[a]	m	The authors
	Conifer, hardwood	9	67	0.70-0.80	1.88-2.29[a]	m	Muss et al. (2011)
	Conifer, hardwood	6	114	0.52-0.55	-5.5-5.0[c]	m	Hawbaker et al. (2010)
	Hardwood	3	33	0.73-0.79	1.82-2.06[a]	m	Popescu et al. (2004)
	Conifer	3	31	0.90-0.97	1.29-2.14[a]	m	Popescu et al. (2004)
	Conifer, hardwood	3	116	0.77-0.92	0.06-0.07[d]	m	Næsset (2004)
	Hardwood	2	49	0.61-0.87	0.09[b]	m	Lim et al. (2003)
CL	Conifer, hardwood	20	60	0.53-0.55	3.36-3.49[a]	m	The authors
	Conifer, hardwood	9	67	0.39-0.48	1.63-1.77[a]	m	Muss et al. (2011)
CW	Conifer, hardwood	20	60	0.51-0.63	2.58-3.06[a]	m	The authors
	Hardwood	3	33	0.33-0.62	1.63-1.69[a]	m	Popescu et al. (2004)
	Conifer	3	31	0.55-0.63	1.27-1.69[a]	m	Popescu et al. (2004)

*Forest structure variables are aboveground biomass (AGB), basal area (BA), diameter at breast height (DBH), tree height (Ht), crown length (CL) and crown width (CW)

[a] Root mean square error (RMSE), values reported in original units

[b] Standard error of residuals, values reported in log transformed units

[c] Range of difference between predictions and observations, values reported in original units

[d] Root mean square error (RMSE), values reported in log transformed units

study, and of these, 20 different tree species dominated composition in at least one of our 50 × 50 m plots, compared to a maximum of 9 dominant species reported in other studies using discrete-return lidar. In addition, human activity and management practices such as regular clearing, trimming and planting activities affect structural patterns of urban forest (Tyrväinen et al. 2003), which may weaken correlations between field measurements and lidar heights, especially if management activities were conducted between lidar acquisition and field sampling.

Uncertainty mapping

To our best knowledge, ours is the first study to explicitly map uncertainty in lidar-derived maps of forest structure in an urban area on a pixel-by-pixel basis (Fig. 4, bottom row). The uncertainties we estimated in this study were only from the statistical models, however, uncertainties in field measurements, remote sensing accuracy and spatial autocorrelation could also contribute to the uncertainties in forest structural variables (Gonzalez et al. 2010). The uncertainty maps identify locations where the maps of structure are less reliable, either because the lidar metrics are beyond the range of those metrics used in the regression analysis, or because the structural variables are estimated to be outside the range of our measurements in plot data. For example, the total uncertainty as a percentage of predicted aboveground biomass was low (10 % - 18 %, i.e. worst-case uncertainties of -8 % to +10 %) in the large patches of forest, compared to high total uncertainty in the edge of forest patches and residential areas (40 % - 50 %, equating to worst-case uncertainties of -22 % to +28 %). The uncertainties in urban forest patches (10 % - 18 %) were higher than that of 1.2 % - 6 % estimated from small-footprint lidar for natural forests in northern California, USA (Gonzalez et al. 2010) because of our weaker aboveground biomass model (R^2 = 0.48 vs. R^2 = 0.80–0.86). Despite higher uncertainties compared to natural forests, our uncertainty maps constitute the first spatially explicit demonstration of uncertainty in forest structure estimates.

On the whole, the highest uncertainties occurred in residential neighborhoods and along forest edges, with uncertainty being negatively correlated with proportion of canopy (PCan in Table 1, r = - 0.4). As such, mixed signals in lidar data yield more variable estimates of the metrics in Table 1. However, large areas of the maps have high confidence, and the areas with lower confidence are known. Uncertainty maps help decision makers to better understand the limitations of the map for management or planning. In addition, they allow urban foresters to target locations for evaluation, monitoring and further measurement to fill gaps in our knowledge.

Carbon stocks in municipalities and implication for management

Carbon storage by urban trees varies significantly among cities, ranging from a high of 5.6 kg/m^2 in the Village of Shorewood Hills, an affluent older neighborhood near the University of Wisconsin campus and hospital, to 1.2 kg/m^2 in City of Verona, a suburban community that has recently experienced considerable new residential housing development. Percent forest cover is one of the main factors affecting carbon storage. In this study, the correlation between carbon storage density and percent forest cover for seven municipalities is 0.96. Aside from percent forest cover, stem diameter distribution is another important factor influencing total carbon stock, with larger diameter trees storing more carbon (Nowak and Crane 2002). It is estimated that the study area stores 27 t C/ha (Table 5), which is comparable to 25.1 t C/ha estimated from field data collected across 10 U.S. cities (Nowak and Crane 2002).

Though total carbon storage per hectare is the lowest in city of Verona, development and land management practices could potentially maximize carbon storage in urban forests. For example, 31 % of Verona is covered by pasture and cultivated crops, converting abandoned grassland and agriculture to forests is a feasible way to increase the carbon sink (Fahey et al. 2010). Other active carbon management includes reducing deforestation for urban development, increasing forest productivity through fertilization at time of planting, insects and competition control, and selecting tree species favorable for storing carbon when planting new trees.

Conclusion

Our goal was to demonstrate that forest structure and associated uncertainties can be mapped using the types of lidar data that are available to most management agencies. At present, due to costs, most urban areas cannot afford dedicated leaf-on lidar for forest characterization. However, most urban areas have access to leaf-off data from past or forthcoming topographic mapping efforts. We present an approach to map forest structure and its uncertainty of estimation in an urban area using leaf-off lidar data that were originally acquired for topographic mapping. Because the available lidar data were opportunistic, and not tuned to our particular application, we used an empirical approach to model and map forest structure. Based on a review of the literature, ours is the first application of using leaf-off discrete lidar to ***map*** forest structure ***as well as*** uncertainty of prediction across an entire urban area, providing initial tabular estimates of total woody biomass and carbon stock by municipality (Table 5). This represents a potentially useful strategy for urban forests management where resources are insufficient for new optimal lidar collection.

Acknowledgments This research was funded by University of Wisconsin-Madison McIntire-Stennis Grant WIS01531. Sincere thanks to Aditya Singh for help in model analysis and Jordan Muss for lidar processing support. Thank you to Marty Dillenburg, Benjamin Spaier, Ryan Sword, Chase Wilson, Austin Pethan and Hannah Hubanks for assistance with fieldwork. We thank Fred Iausly and Kevin Connors (Dane County), Marla Eddy and Dave Davis (City of Madison), and Kirk Contrucci (Ayres Associates) for assistance in procuring lidar data. We also thank Matt Garcia and other members of Townsend Lab for helpful suggestions.

References

3DEP (2014) 3D elevation program. U.S. Geological Survey. http://nationalmap.gov/3DEP Accessed 15 January 2015

Akbari H, Pomerantz M, Taha H (2001) Cool surfaces and shade trees to reduce energy use and improve air quality in urban areas. Sol Energy 70(3):295–310. doi:10.1016/s0038-092x(00)00089-x

Alvey AA (2006) Promoting and preserving biodiversity in the urban forest. Urban Forestry Urban Greening 5:195–201. doi:10.1016/j.ufug.2006.09.003

Anderson ES, Thompson JA, Austin RE (2005) LIDAR density and linear interpolator effects on elevation estimates. Int J Remote Sens 26(18):3889–3900. doi:10.1080/01431160500181671

Anderson RS, Bolstad PV (2013) Estimating aboveground biomass and average annual wood biomass increment with airborne leaf-on and leaf-off LiDAR in Great Lakes Forest types. North J Appl For 30(1):16–22. doi:10.5849/njaf.12-015

Bolund P, Hunhammar S (1999) Ecosystem services in urban areas. Ecol Econ 29:293–301

Bortolot ZJ (2006) Using tree clusters to derive forest properties from small footprint lidar data. Photogramm Eng Remote Sens 40351:1389–1397

Brandtberg T, Warner TA, Landenberger RE, McGraw JB (2003) Detection and analysis of individual leaf-off tree crowns in small footprint, high sampling density lidar data from the eastern deciduous forest in North America. Remote Sens Environ 85(3):290–303. doi:10.1016/s0034-4257(03)00008-7

Cairns MA, Brown S, Helmer EH, Baumgardner GA (1997) Root biomass allocation in the world's upland forests. Oecologia 111(1):1–11. doi:10.1007/s004420050201

Day SD, Wiseman PE, Dickinson SB, Harris JR (2010) Tree root ecology in the urban environment and implications for a sustainable rhizosphere. Arboricult Urban For 36:193–205

ESRI (2012) ArcGIS desktop, version 10.1 Environmental Systems Research Institute, Redlands, CA

Fahey TJ, Woodbury PB, Battles JJ, Goodall CL, Hamburg SP, Ollinger SV, Woodall CW (2010) Forest carbon storage: ecology, management, and policy. Front Ecol Environ 8(5):245–252. doi:10.1890/080169

Farid A, Goodrich DC, Bryant R, Sorooshian S (2008) Using airborne lidar to predict leaf area index in cottonwood trees and refine riparian water-use estimates. J Arid Environ 72:1–15. doi:10.1016/j.jaridenv.2007.04.010

Frazer GW, Magnussen S, Wulder MA, Niemann KO (2011) Simulated impact of sample plot size and co-registration error on the accuracy and uncertainty of LiDAR-derived estimates of forest stand biomass. Remote Sens Environ 115(2):636–649. doi:10.1016/j.rse.2010.10.008

García M, Riaño D, Chuvieco E, Danson FM (2010) Estimating biomass carbon stocks for a Mediterranean forest in Central Spain using LiDAR height and intensity data. Remote Sens Environ 114:816–830. doi:10.1016/j.rse.2009.11.021

Gleason CJ, Im J (2012) Forest biomass estimation from airborne LiDAR data using machine learning approaches. Remote Sens Environ 125:80–91. doi:10.1016/j.rse.2012.07.006

Gonzalez P, Asner GP, Battles JJ, Lefsky MA, Waring KM, Palace M (2010) Forest carbon densities and uncertainties from Lidar, quick bird, and field measurements in California. Remote Sens Environ 114(7):1561–1575. doi:10.1016/j.rse.2010.02.011

Grosenbaugh LR (1952) Plotless timber estimates – new, fast, easy. J For 50:32–37

Grosenbauch LR (1958) Point-sampling and line-sampling: probability theory, geometric implications, synthesis. USDA Forest Service Southern Experiment Station Occasional Paper 160:1–34

Gu (2015) Mapping forest structure, species gradients and growth in an urban area using lidar and hyperspectral imagery. The University of Wisconsin-Madison Dissertation, ProQuest Dissertations and Theses Order No 3680343:9–65

Gu H, Singh A, Townsend PA (2015) Detection of gradients of forest composition in an urban area using imaging spectroscopy. Remote Sens Environ 167:168–180. doi:10.1016/j.rse.2015.06.010

Hawbaker TJ, Gobakken T, Lesak A, Tromborg E, Contrucci K, Radeloff V (2010) Light detection and ranging-based measures of mixed hardwood forest structure. For Sci 56(3):313–326

Hodgson ME, Jensen J, Raber G, Tullis J, Davis BA, Thompson G, Schuckman K (2005) An evaluation of lidar-derived elevation and terrain slope in leaf-off conditions. Photogramm Eng Remote Sens 71(7):817–823

Hope D, Gries C, Zhu WX, Fagan WF, Redman CL, Grimm NB, Nelson AL, Martin C, Kinzig A (2003) Socioeconomics drive urban plant diversity. Proc Natl Acad Sci U S A 100:8788–8792

Hudak AT, Crookston NL, Evans JS, Hall DE, Falkowski MJ (2008) Nearest neighbor imputation of species-level, plot-scale forest structure attributes from LiDAR data. Remote Sens Environ 112(5):2232–2245. doi:10.1016/j.rse.2007.10.009

Hyde P, Dubayah R, Walker W, Blair JB, Hofton M, Hunsaker C (2006) Mapping forest structure for wildlife habitat analysis using multi-sensor (LiDAR, SAR/InSAR, ETM+, Quickbird) synergy. Remote Sens Environ 102:63–73. doi:10.1016/j.rse.2006.01.021

Hyde P, Nelson R, Kimes D, Levine E (2007) Exploring LiDAR–RaDAR synergy—predicting aboveground biomass in a southwestern ponderosa pine forest using LiDAR, SAR and InSAR. Remote Sens Environ 106:28–38. doi:10.1016/j.rse.2006.07.017

Jenkins JC, Chojnacky DC, Heath LS, Birdsey RA (2004) Comprehensive database of diameter-based biomass regressions for north American tree species. USDA Forest Service Northeastern Research Station General Technical Report NE-319:1–45

Kellndorfer J, Walker W, Kirsch K, Fiske G, Bishop J, Lapoint L, Hoppus M, Westfall J (2013) NACP Aboveground biomass and carbon baseline data, V.2 (NBCD 2000), U.S.A., 2000. Oak Ridge National Laboratory Distributed Active Archive Center for Biogeochemical Dynamics. doi:10.3334/ornldaac/1161

Korhonen L, Korpela I, Heiskanen J, Maltamo M (2011) Airborne discrete-return LIDAR data in the estimation of vertical canopy cover, angular canopy closure and leaf area index. Remote Sens Environ 115:1065–1080. doi:10.1016/j.rse.2010.12.011

Lefsky MA, Cohen WB, Parker GG, Harding DJ (2002) Lidar remote sensing for ecosystem studies. Bioscience 52:19–30

Lesak AA, Radeloff VC, Hawbaker TJ, Pidgeon AM, Gobakken T, Contrucci K (2011) Modeling forest songbird species richness using LiDAR-derived measures of forest structure. Remote Sens Environ 115(11):2823–2835. doi:10.1016/j.rse.2011.01.025

Lim K, Treitz P, Baldwin K, Morrison I, Green J (2003) Lidar remote sensing of biophysical properties of tolerant northern hardwood forests. Can J Remote Sens 29:658–678

Lovasi GS, O'Neil-Dunne JPM, Lu JWT, Sheehan D, Perzanowshi MS, MacFaden SW, King KL, Matte T, Miller RL, Hoepner LA, Perera FP, Rundle A (2013) Urban tree canopy and asthma, wheeze, rhinitis, and allergic sensitization to tree pollen in a New York City birth cohort. Environ Health Perspect 121:494–500

Lu DS, Chen Q, Wang GX, Moran E, Batistella M, Zhang M, Laurin GV, Saah D, Zhang MZ (2012) Aboveground forest biomass estimation with landsat and LiDAR data and uncertainty analysis of the estimates. International Journal of Forestry Research 2012:436537 Article ID 436537

McPherson EG, Nowak D, Heisler G, Grimmond S, Souch C, Grant R, Rowntree R (1997) Quantifying urban forest structure, function, and value: the Chicago urban Forest climate project. Urban Ecosystems 1(1):49–61. doi:10.1023/a:1014350822458

Moskal LM, Zheng G (2012) Retrieving Forest inventory variables with terrestrial laser scanning (TLS) in urban heterogeneous Forest. Remote Sens 4(1):1–20

Morsdorf F, Kötz B, Meier E, Itten KI, Allgower B (2006) Estimation of LAI and fractional cover from small footprint airborne laser scanning data based on gap fraction. Remote Sens Environ 104:50–61. doi:10.1016/j.rse.2006.04.019

Muss JD, Mladenoff DJ, Townsend PA (2011) A pseudo-waveform technique to assess forest structure using discrete lidar data. Remote Sens Environ 115:824–835. doi:10.1016/j.rse.2010.11.008

Myeong S, Nowak DJ, Duggin MJ (2006) A temporal analysis of urban forest carbon storage using remote sensing. Remote Sens Environ 101:277–282. doi:10.1016/j.rse.2005.12.001

Nowak DJ, Crane DE (2002) Carbon storage and sequestration by urban trees in the USA. Environ Pollut 116:381–389

Nowak DJ, Greenfield EJ, Hoehn RE, Lapoint E (2013) Carbon storage and sequestration by trees in urban and community areas of the United States. Environ Pollut 178:229–236. doi:10.1016/j.envpol.2013.03.019

Næsset E (2004) Practical large-scale forest stand inventory using a small-footprint airborne scanning laser. Scand J For Res 19:164–179. doi:10.1080/02827580310019257

Næsset E (2005) Assessing sensor effects and effects of leaf-off and leaf-on canopy conditions on biophysical stand properties derived from small-footprint airborne laser data. Remote Sens Environ 98(2-3):356–370. doi:10.1016/j.rse.2005.07.012

Omasa K, Hosoi F, Uenishi TM, Shimizu Y, Akiyama Y (2008) Three-dimensional modeling of an urban park and trees by combined airborne and portable on-ground scanning LIDAR remote sensing. Environ Model Assess 13(4):473–481

Poland TM, McCullough DG (2006) Emerald ash borer: invasion of the urban forest and the threat to North America's ash resource. J For 104(3):118–124

Popescu SC, Wynne RH, Scrivani JA (2004) Fusion of small-footprint lidar and multispectral data to estimate plot-level volume and biomass in deciduous and pine forests in Virginia, USA. For Sci 50(4):551–565

R Development Core Team (2013) A language and environment for statistical computing. R Foundation for Statistical Computing, Vienna, Austria

Savard J-PL, Clergeau P, Mennechez G (2000) Biodiversity concepts and urban ecosystems. Landsc Urban Plan 48:131–142

Shrestha R, Wynne RH (2012) Estimating biophysical parameters of individual trees in an urban environment using small footprint discrete-return imaging lidar. Remote Sens 4(2):484–508

Swatantran A, Dubayah R, Roberts D, Hofton M, Blair JB (2011) Mapping biomass and stress in the sierra Nevada using lidar and hyperspectral data fusion. Remote Sens Environ 115:2917–2930. doi:10.1016/j.rse.2010.08.027

Townsend PA (2002) Relationships between forest structure and the detection of flood inundation in forested wetlands using C-band SAR. Int J Remote Sens 23:443–460

Tyrväinen L, Silvennoinen H, Kolehmainen O (2003) Ecological and aesthetic values in urban forest management. Urban For Urban Green 1:135–149

Wasser L, Day R, Chasmer L, Taylor A (2013) Influence of vegetation structure on lidar-derived canopy height and fractional cover in forested riparian buffers during leaf-off and leaf-on conditions. PLoS One 8(1):e54776